Supporting Information

Ultrahigh Energy Storage Density and Efficiency in Facile Dual-Layered PVDF/PEI-Based Nanocomposites via Electrical/Thermal Synergistic Effect

Yanlong Ma, [a] Ying Lin, *[a] Yongjing Zhang, [a] Yongzhen Ma, [a] Binglong Zheng, [a] Zhener Dang, [a] Qibin Yuan *[b] and Haibo Yang *[a]

[a] Shaanxi Key Laboratory of Green Preparation and Functionalization for Inorganic Materials, School of Materials Science and Engineering, Shaanxi University of Science and Technology, Xi'an 710021, China.

[b] School of Electronic Information & Artificial Intelligence, Shaanxi University of Science and Technology, Xi'an 710021, China.

* Corresponding Author.

E-mail addresses: linying@sust.edu.cn (Ying Lin)

yuanqibin-sust@163.com (Qibin Yuan)

yanghaibo@sust.edu.cn (Haibo Yang)

Supplemented experiments

Materials: Analytical-grade Polyetherimide (PEI) was provided by SABIC, Co., Ltd. Poly (vinylidene fluoride) (PVDF) was supplied by Arkema Co., LLC. Boron nitride nanosheets (BNNSs) powder with average particle size of 300 nm was provided by Sigma Aldrich Co., Ltd. N-methyl-2-pyrrolidone (NMP), Isopropanol (IPA), and N, N-dimethylformamide (DMF) were bought from Sinopharm Chemical Reagent Co., Ltd. Other chemicals and reagents were obtained from Tianjin Fuyu Fine Chemical Co., Ltd.

Preparation of BNNSs: BNNSs were prepared through a liquid phase exfoliation method. Initially, BNNSs powder was added to an IPA solution with a volume percentage of 50%. This mixture was alternately subjected to a sonication bath for 1 h and mechanically stirred for 1 h, repeating this process six consecutive times. Then, the processed suspension was centrifuged at 3000 rpm for 10 min and the supernatant was collected. Finally, the BNNSs were collected via filtration, followed by a vacuum drying process for 12 h at 60 °C to remove any excess solvent.

Fabrication of the F-EB$_5$ composites: 1.4 g PEI particles were added to the NMP solution and stirred at 600 rpm for 18 h at 60 °C to obtain a dissolved and clarified PEI solution A. 1.2 g PVDF powders were added to the DMF solution and stirred at 600 rpm for 12 h at 45 °C to obtain a dissolved and clarified PVDF solution B. Calculated amount of BNNSs were added to the IPA solution and stirred at 600 rpm for 18 h at 25 °C to obtain a dispersed BNNSs suspension C. The composites were produced using a solution casting method, with squeegee height set at 12 μm, 13 μm, 13 μm, and 15 μm, respectively. Firstly, the solution A was coated on the ITO glass plate, followed by the suspension C, and finally the solution A was coated on the top side. The obtained underlying PEI-BNNS-PEI composites were initially placed in an

oven at 90 °C for 18 h to remove the solvent. Subsequently, the solution B was coated on the dried film and then placed in an oven at 60 °C for 14 h to remove the solvent. Thereafter, to achieve dense composites, the samples were subjected to oven heating at 200 °C for 9 min, and then cooled in an ice-water mixture. Finally, the samples were heated in an oven at 60 °C for 12 h to facilitate water evaporation.

Fabrication of the F-EB$_5$-C composites: 1.2 g PEI particles were added to the NMP solution and stirred at 600 rpm for 18 h at 60 °C to obtain a dissolved and clarified PEI solution A. 1.2 g PVDF powders were added to the DMF solution and stirred at 600 rpm for 12 h at 45 °C to obtain a dissolved and clarified PVDF solution B. 1.2 g PEI particles and calculated amount of BNNSs powders were added to the NMP solution and stirred at 600 rpm for 18 h at 60 °C to obtain a dissolved and dispersed PEI/BNNSs solution. Subsequently, the solution C was subjected to ultrasonic treatment for 1 h to obtain a stable PEI/BNNSs suspension C. The composites were produced using a solution casting method, with squeegee height set at 11 μm, 12 μm, 13 μm, and 15 μm, respectively. Firstly, the solution A was coated on the ITO glass plate, followed by the suspension C., and finally the solution A was coated on the top side. The obtained underlying PEI-BNNS/PEI-PEI composite was initially placed in an oven at 90 °C for 18 h to remove the solvent. Subsequently, the solution C was coated on the dried composite and then placed in an oven at 60 °C for 14 h to remove the solvent. Thereafter, to achieve dense composites, the samples were subjected to oven heating at 200 °C for 9 min, and then cooled in an ice-water mixture. Finally, the samples were heated in an oven at 60 °C for 12 h to facilitate water evaporation.

Fabrication of the F-EB$_5$-D composites: 1.6 g PEI particles and calculated amount of BNNSs powders were added to the NMP solution and stirred at 600 rpm for 18 h at 60 °C to obtain a dissolved and dispersed PEI/BNNSs solution. Subsequently, the solution was subjected to ultrasonic treatment for 1 h to obtain a stable PEI/BNNSs suspension A. 1.2 g PVDF powders

were added to the DMF solution and stirred at 600 rpm for 12 h at 45 °C to obtain a dissolved and clarified PVDF solution B. The composites were produced using a solution casting method, with squeegee height set at 13 μm and 15 μm. Firstly, the suspension A was coated on the ITO glass plate to obtain BNNSs/PEI. The obtained underlying PEI-BNNSs/PEI-PEI composite was initially placed in an oven at 90 °C for 18 h to remove the solvent. Subsequently, the solution B was coated on the dried composite and then placed in an oven at 60 °C for 14 h to remove the solvent. Thereafter, to achieve dense composites, the samples were subjected to oven heating at 200 °C for 9 min, and then cooled in an ice-water mixture. Finally, the samples were heated in an oven at 60 °C for 12 h to facilitate water evaporation.

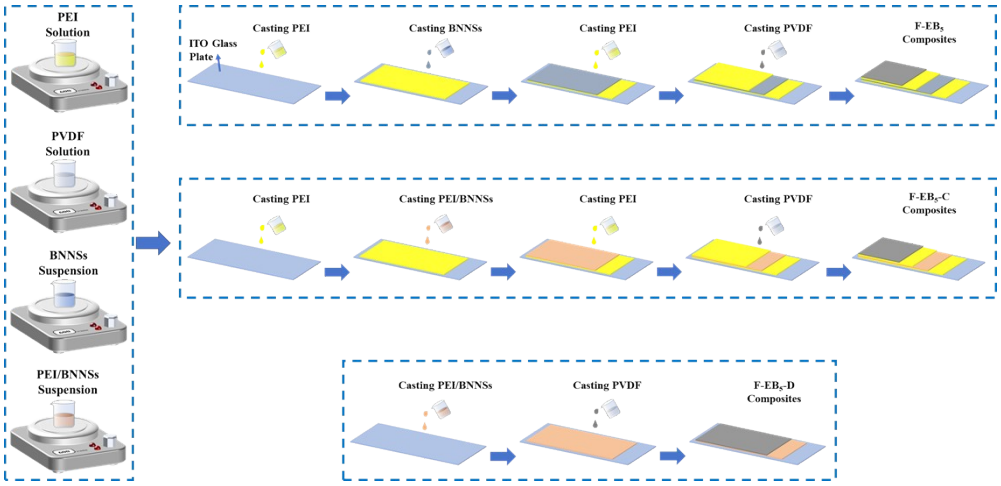

Fig. S1 Fabrication of composites with different structures.

Measurement of dielectric and energy storage characteristics: The dielectric tests of the composites were performed using an impedance analyzer (E4990A, Agilent, Palo Alto, CA) to determine the dielectric constant and dielectric loss of the composites in the frequency range from 1 kHz to 10 MHz. The energy storage properties of the composite films were determined using a ferroelectric test system (Premier II, Radiant, USA), in which the composites were immersed in silicone oil and characterized by a hysteresis (*P*-*E*) loop at a frequency of 100 Hz.

Before measurements, the gold electrodes with a diameter of 2 mm were coated on both sides of the composites using an auto fine coater (JFC-1 calculated, JEOL, Ltd., Japan).

Finite element analysis calculations of electric potentials and electric trees: To better investigate the influence of various components on the energy storage capabilities of composites, finite element simulations were utilized for studying the distributions of electric potential and electrical breakdown process of such composites. A series of two-dimensional computational models measuring 13 μm × 18 μm were created, with the permittivity of PVDF, PEI, and BNNSs being 7.57, 3.25, and 2.2, respectively. The breakdown process was studied according to the following Eq. (S1):

$$p\left(i', j' \rightarrow i, j\right) = \frac{(\phi_{i', j'} - \phi_{i, j} - \phi)^m}{\sum (\phi_{i', j'} - \phi_{i, j} - \phi)^m} + (\phi_{i', j'} - \phi_{i'', j''} - \phi)^m - \text{loss} \tag{S1}$$

where ϕ is the electric potential for all the lattice points, i,j, i',j', and i'',j'' represent the discharged point, probable point, and linked point, respectively. m is the fractal dimension. loss represents the evolve loss of tip electric tree channels.

Finite element analysis calculations of heat transfer process: To establish the relationship between structure and heat distribution of composites, finite element simulations were utilized for studying the heat transfer process of such composites. A cylindrical 3D model of the composite material was constructed, with the upper and lower ends of the cylinder representing the inner and outer surfaces of the composite, respectively. The outer surface of the model was heated through natural convection using hot air, with the air temperature set at 150 °C. The heat transfer process was studied according to the following Eq. (S2):

$$\rho C_{\mathrm{P}} \frac{\partial T}{\partial t} + \rho C_{\mathrm{P}} \boldsymbol{v} \cdot \nabla T + \nabla \cdot \mathbf{q} = Q + Q_{\mathrm{ted}} \tag{S2}$$

Where ρ, C_p, T, t, $\boldsymbol{v}$, $\boldsymbol{q}$, and Q represent the density, constant pressure heat capacity, temperature, time duration, velocity vector, conducted heat flux vector, and system absorbs heat, respectively.

Supplemented results

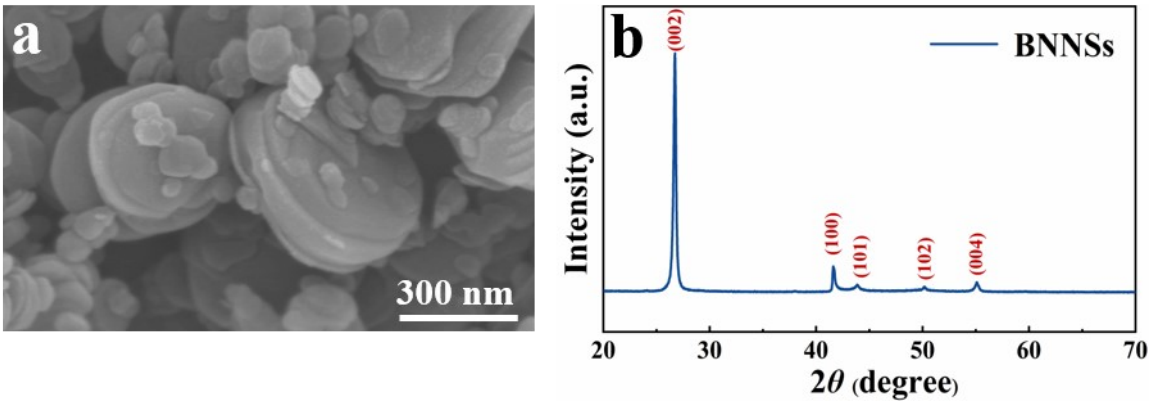

Fig. S2 (a) SEM image and (b) XRD pattern of BNNSs.

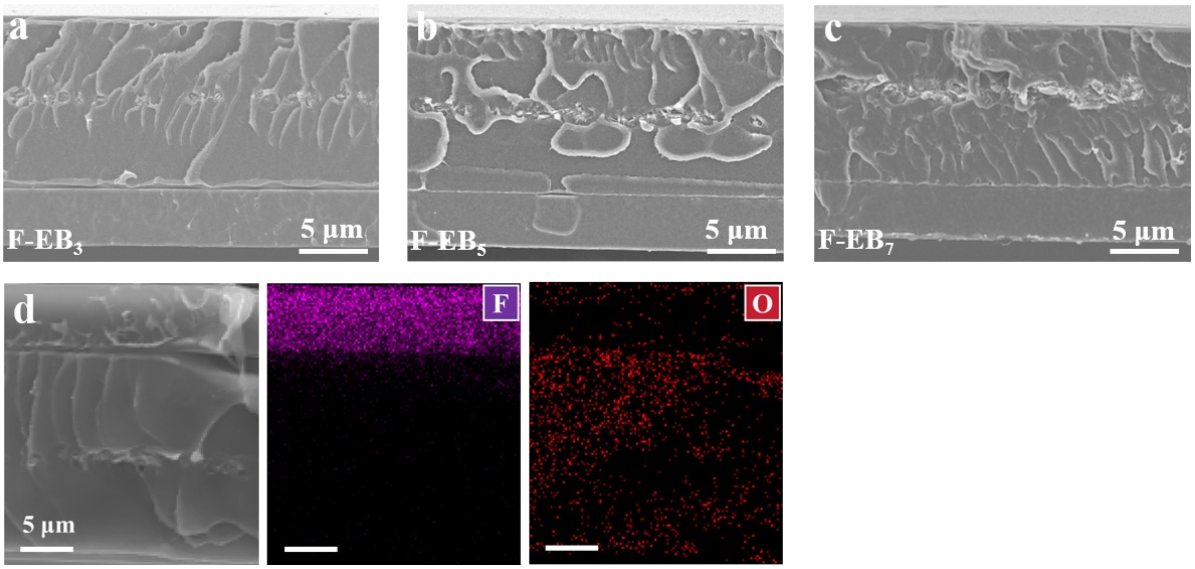

Fig. S3 Cross-sectional SEM images of (a) F-EB_3, (b) F-EB_5, and (c) F-EB_7 composites. (d) EDX analyses on cross-section of F-EB_5 composite.

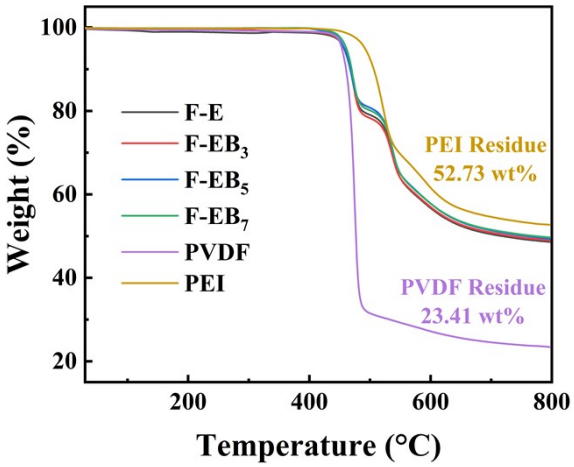

Fig. S4 TG analyses on each polymer dielectric.

Table S1 Mass and volume fractions of each component in composites.

Sample	Residue (%)	PEI (wt%)	PEI (vol%)	PVDF (wt%)	PVDF (vol%)	BNNSs (wt%)	BNNSs (vol%)
F-E	48.62	85.99	89.20	14.01	10.80	0	0
F-EB$_3$	48.99	85.33	88.73	13.90	10.80	0.74	0.47
F-EB$_5$	49.38	84.70	88.31	13.80	10.75	1.49	0.94
F-EB$_7$	49.70	84.17	87.95	13.71	10.70	2.13	1.35

At 800 °C, the residuals are 52.73 wt% for PEI and 23.41 wt% for PVDF, while the BNNSs do not decompose. Thermogravimetric (TG) analysis showed that the mass fractions of PEI and PVDF in F-E was 85.99 wt% and 14.01 wt%, respectively. The BNNSs content increased to 0.74 wt% in F-EB$_3$, 1.49 wt% in F-EB$_5$, and 2.13 wt% in F-EB$_7$. Due to different amounts of BNNSs added, the mass fractions and volume fractions of PEI and PVDF in the F-EB structural composites varied slightly, with PEI at ± 1.16 wt% versus ± 0.78 vol%, and PVDF at ± 0.19 wt% versus ± 0.10 vol%, respectively.

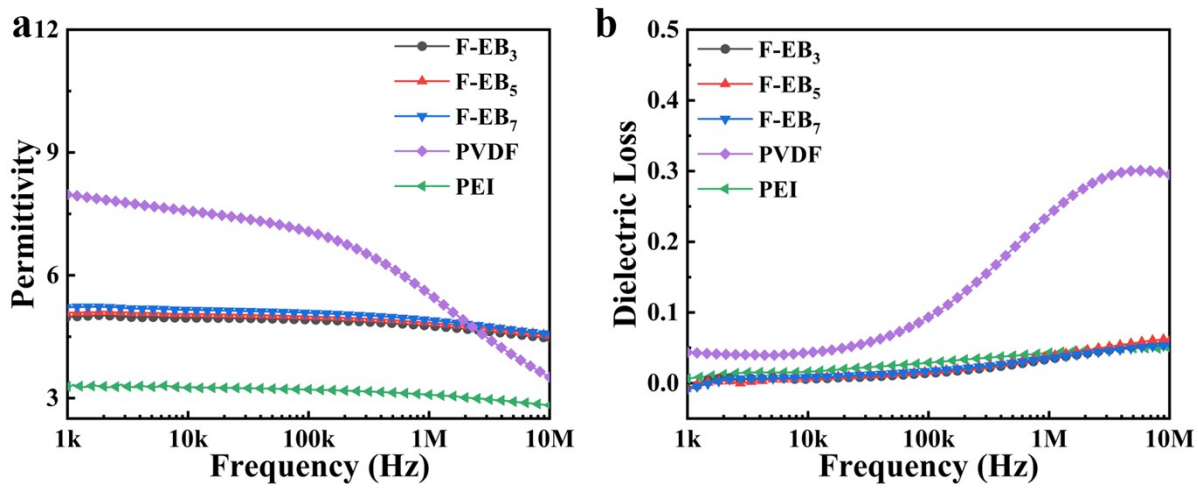

Fig. S5 Frequency dependence of (a) permittivity and (b) dielectric loss of the PEI, PVDF, and each component of F-EB composites.

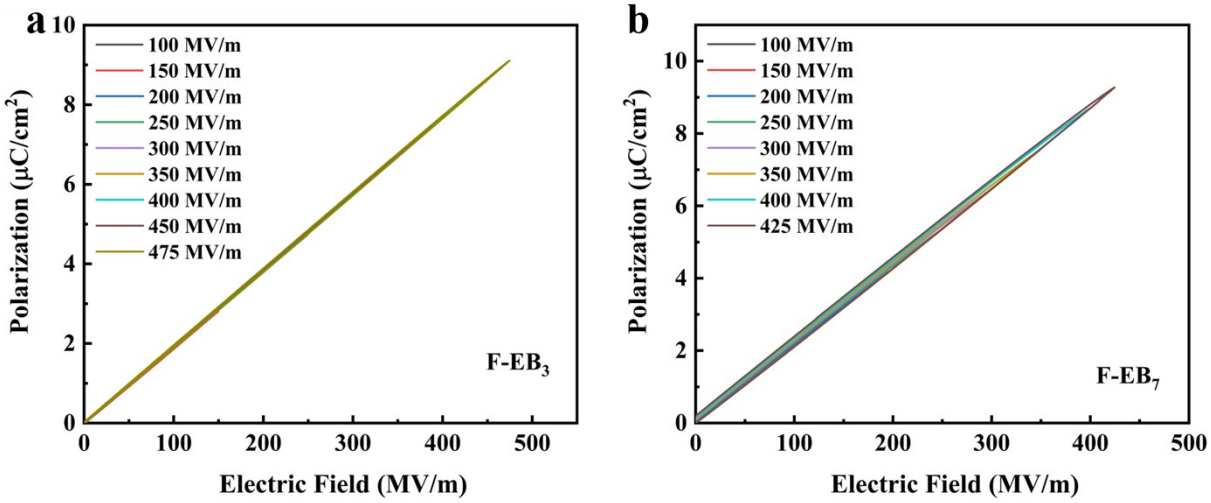

Fig. S6 *P*-*E* loops of (a) F-EB$_3$ and (b) F-EB$_7$ composites under different electric fields.

The energy storage density (U_e) and efficiency (η) of the composite films were calculated through the *P*-*E* loops according to Eq. (S3) and (S4):

$$U_e = \int_{P_r}^{P_{max}} E\mathrm{d}P \tag{S3}$$

$$\eta = \frac{U_e}{\int_0^{P_{max}} E\mathrm{d}P} \tag{S4}$$

where P_{max}, P_r, and E represent maximum polarization, remnant polarization, and electric filed strength, respectively.

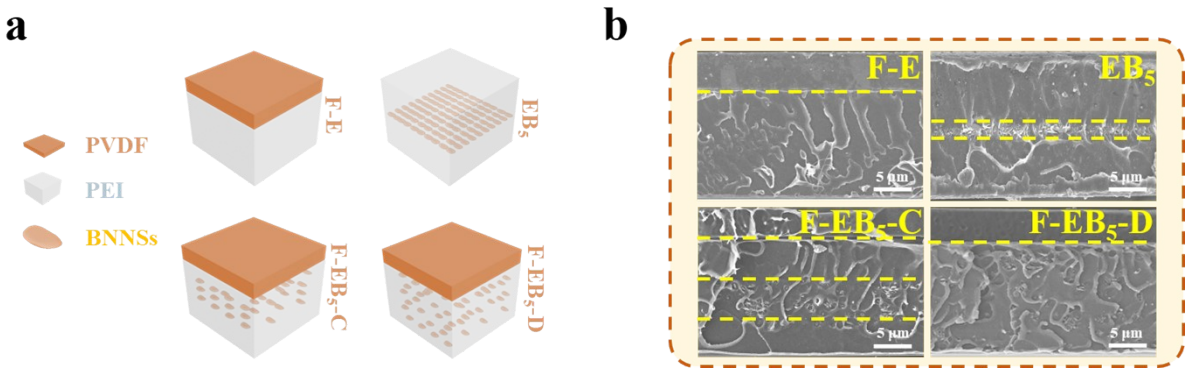

Fig. S7 (a) Schematic illustration and (b) cross-section SEM images of each structural composites.

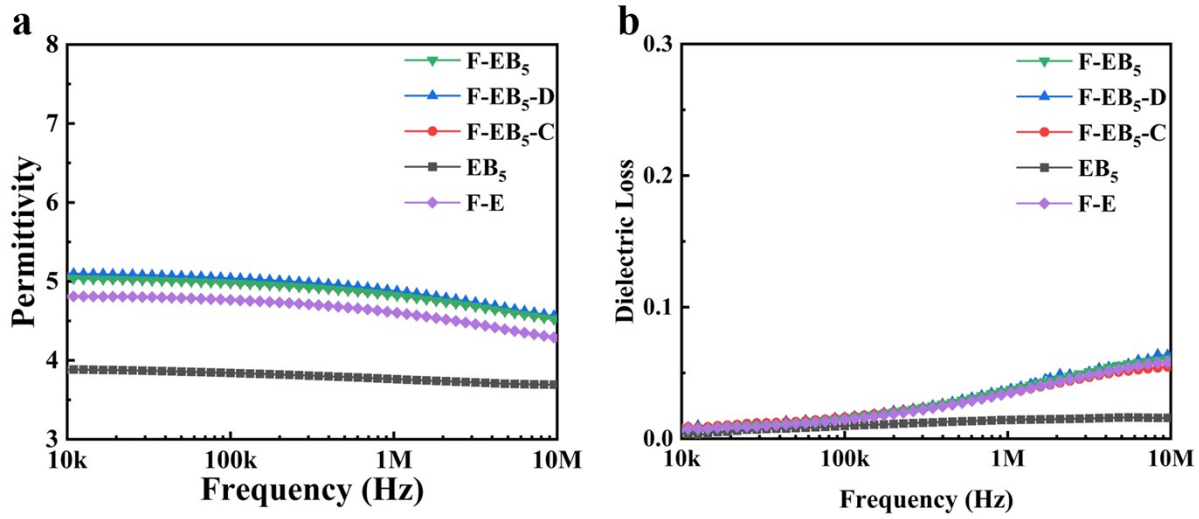

Fig. S8 Frequency dependence of (a) permittivity and (b) dielectric loss of F-EB_5, F-EB_5-D, F-EB_5-C, EB_5, and F-E composites.

The Lichtenecker equation:

$$\varepsilon^{-1} = x_1\varepsilon_1^{-1} + x_2\varepsilon_2^{-1} \tag{S5}$$

where ε is the relative permittivity of F-EB_5 composites, x_1 and ε_1 are the volume fraction and relative permittivity of EB_5 composites, and x_2 and ε_2 are the volume fraction and relative permittivity of PVDF. In the Eq. (S5), ε is determined by using x_1, ε_1, x_2, and ε_2 from the experimental data.

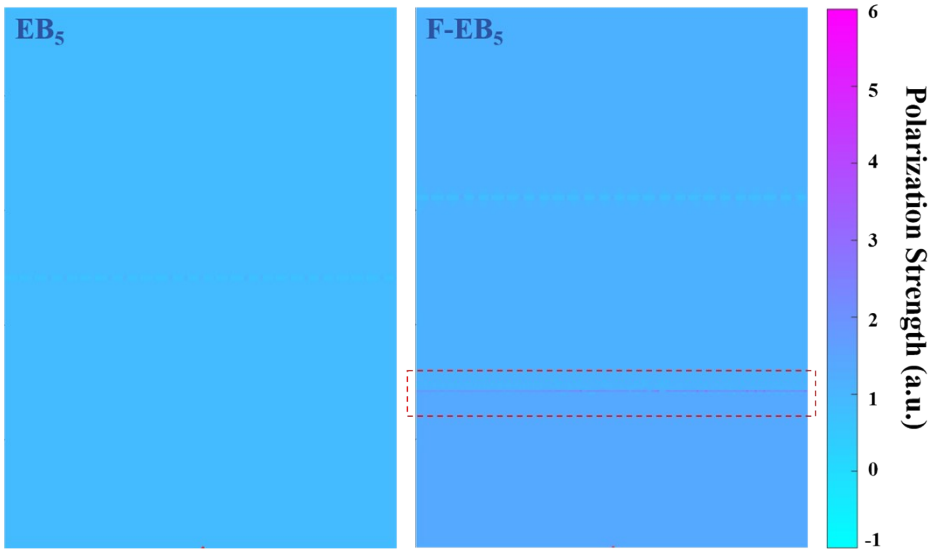

Fig. S9 Polarization intensity distribution of EB_5 and F-EB_5 cross-sections (interface in red wireframe).

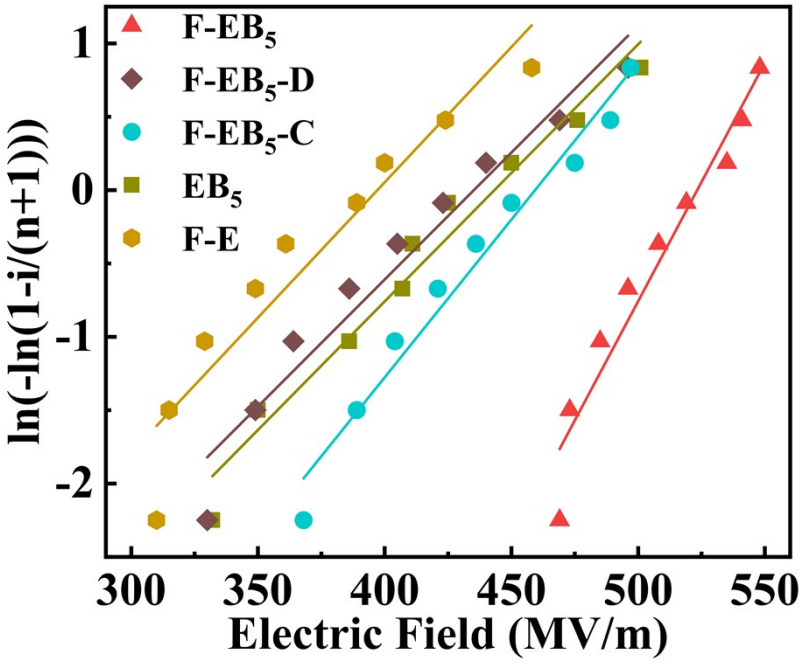

Fig. S10 Weibull distribution of F-EB_5, F-EB_5-D, F-EB_5-C, EB_5, and F-E composites.

The Weibull distribution is defined in Eq. (S6):

$$P(E) = 1 - \exp\left[- \left(E/E_b\right)^{\beta}\right] \quad \text{(S6)}$$

where $P(E)$ represents the cumulative probability of electrical failure, E denotes the measured breakdown field strength in the experiment. E_b indicates the breakdown field strength at a cumulative probability of 63.2%, while β serves as a revelation of the dispersion of the measured breakdown field strength.

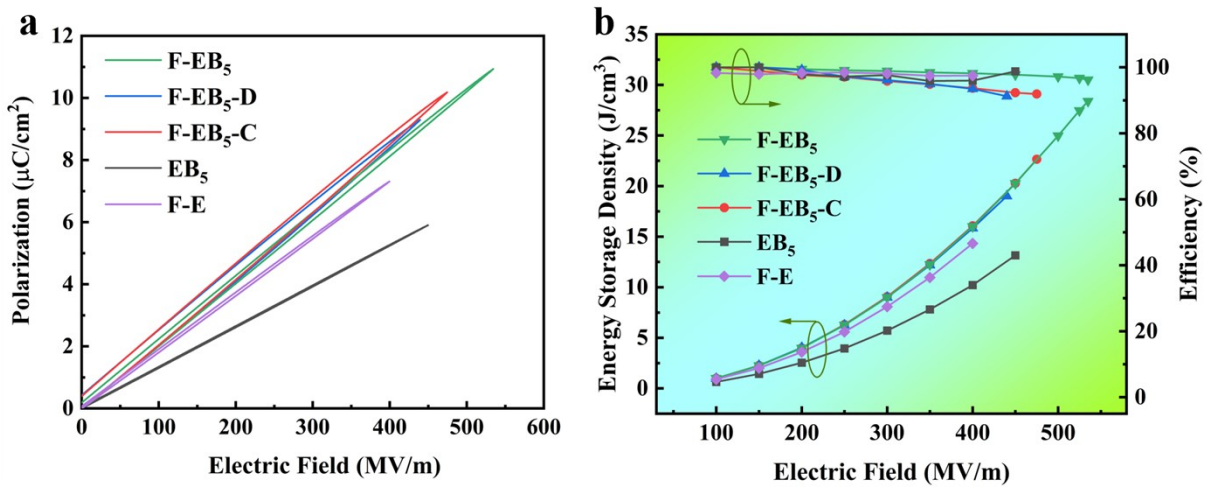

Fig. S11 (a) *P-E* loops and (b) U_e and η under different electric fields of the F-EB_5, F-EB_5-D, F-EB_5-C, EB_5, and F-E composites.

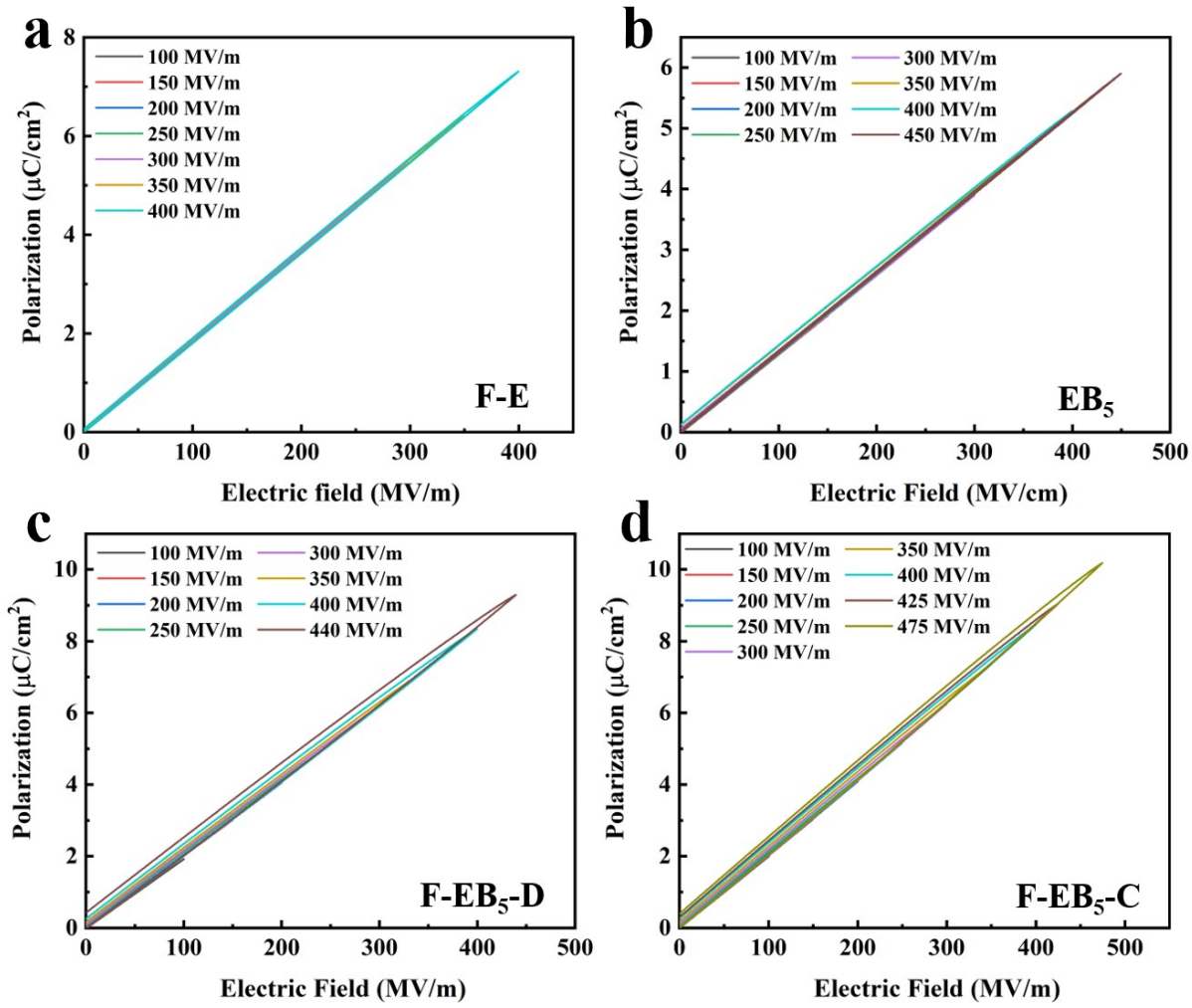

Fig. S12 *P-E* loops of (a) F-E, (b) EB_5, (c) F-EB_5-D, and (d) F-EB_5-C under different electric fields.

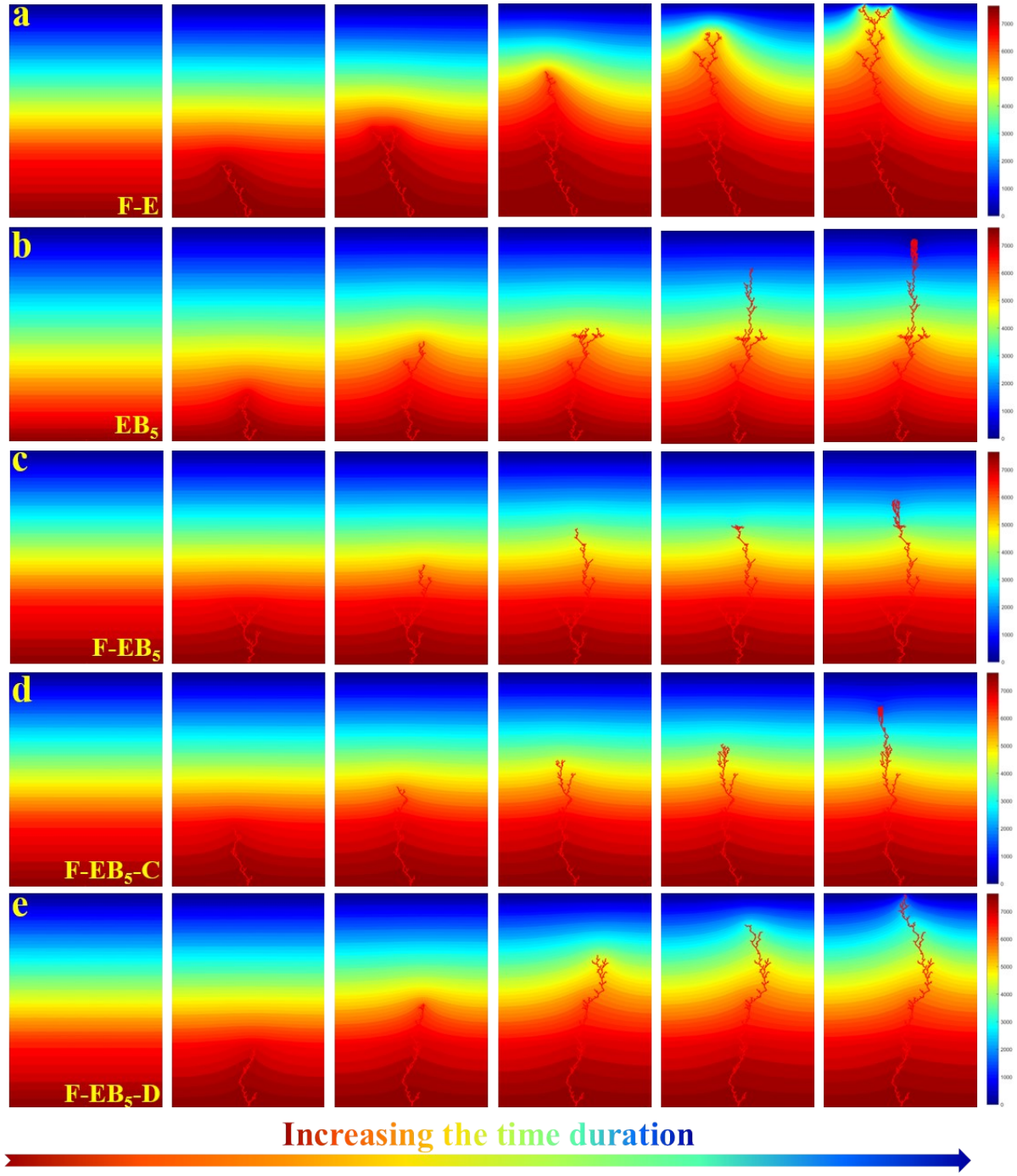

Fig. S13 The electric potential distribution and electric trees evolution of (a) F-E, (b) EB_5, (c) F-EB_5, (d) F-EB_5-C, and (e) F-EB_5-D composites.

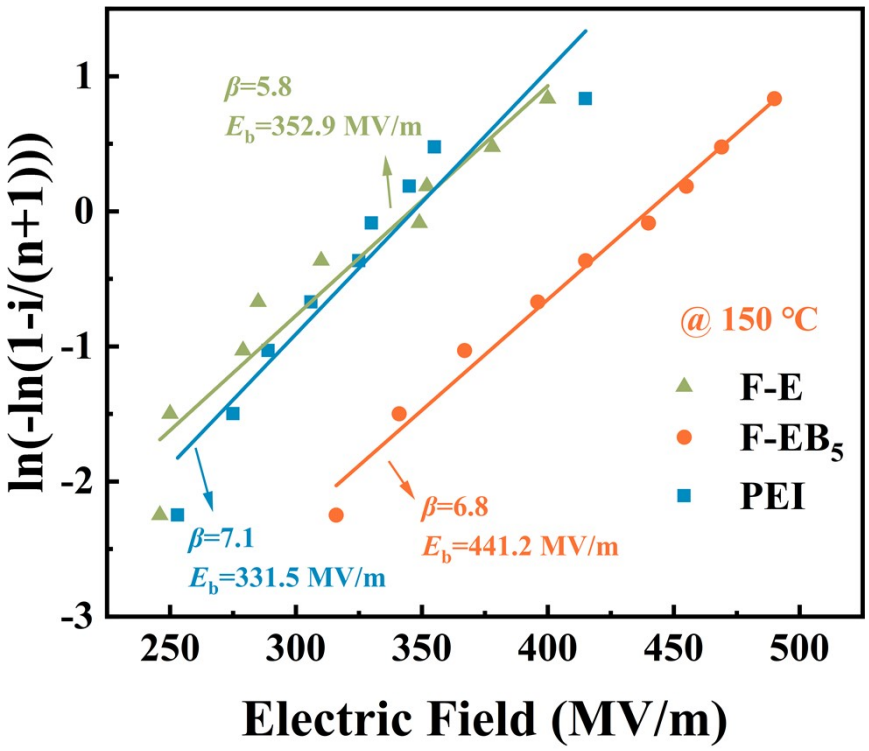

Fig. S14 Weibull distribution of PEI, F-E, and F-EB_5 composites at 150 °C.

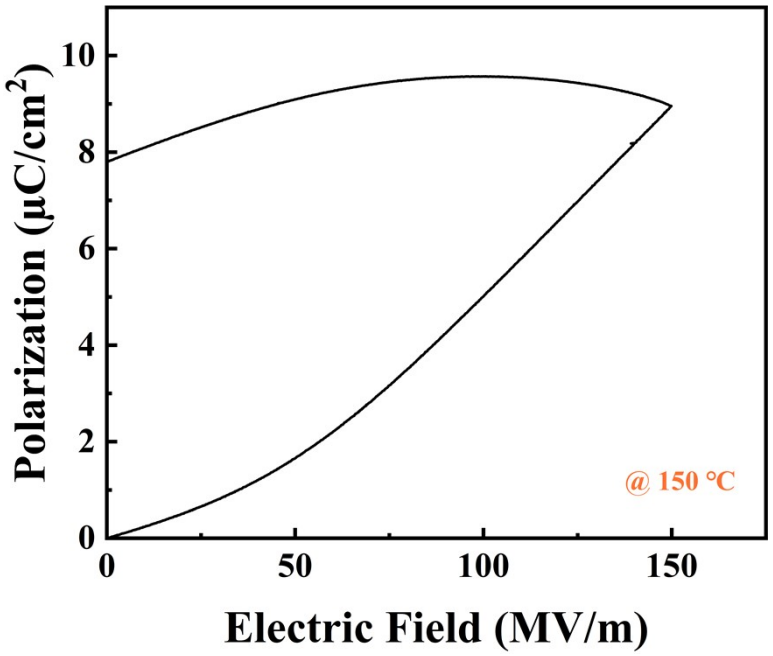

Fig. S15 *P-E* loop of PVDF at 150 °C.

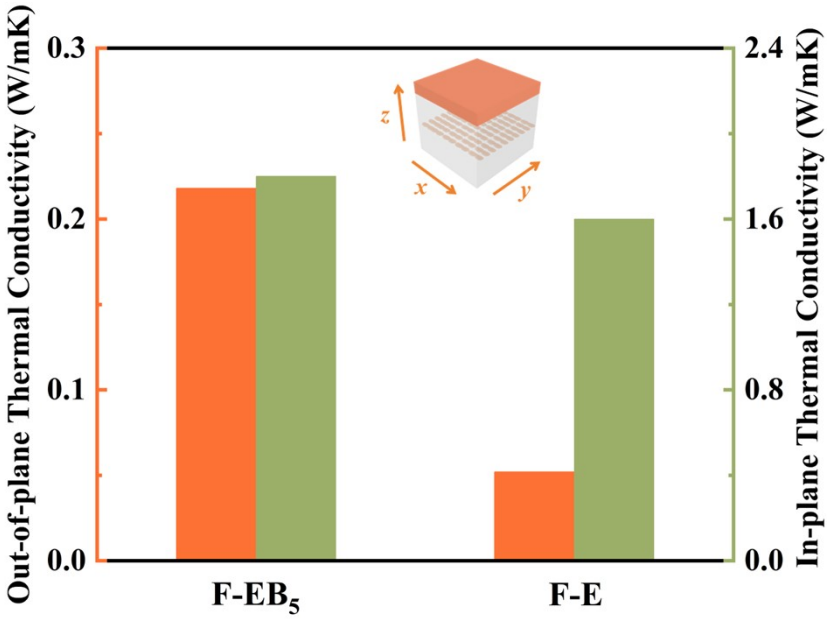

Fig. S16 Thermal conductivity of F-EB_5 and F-E composites.

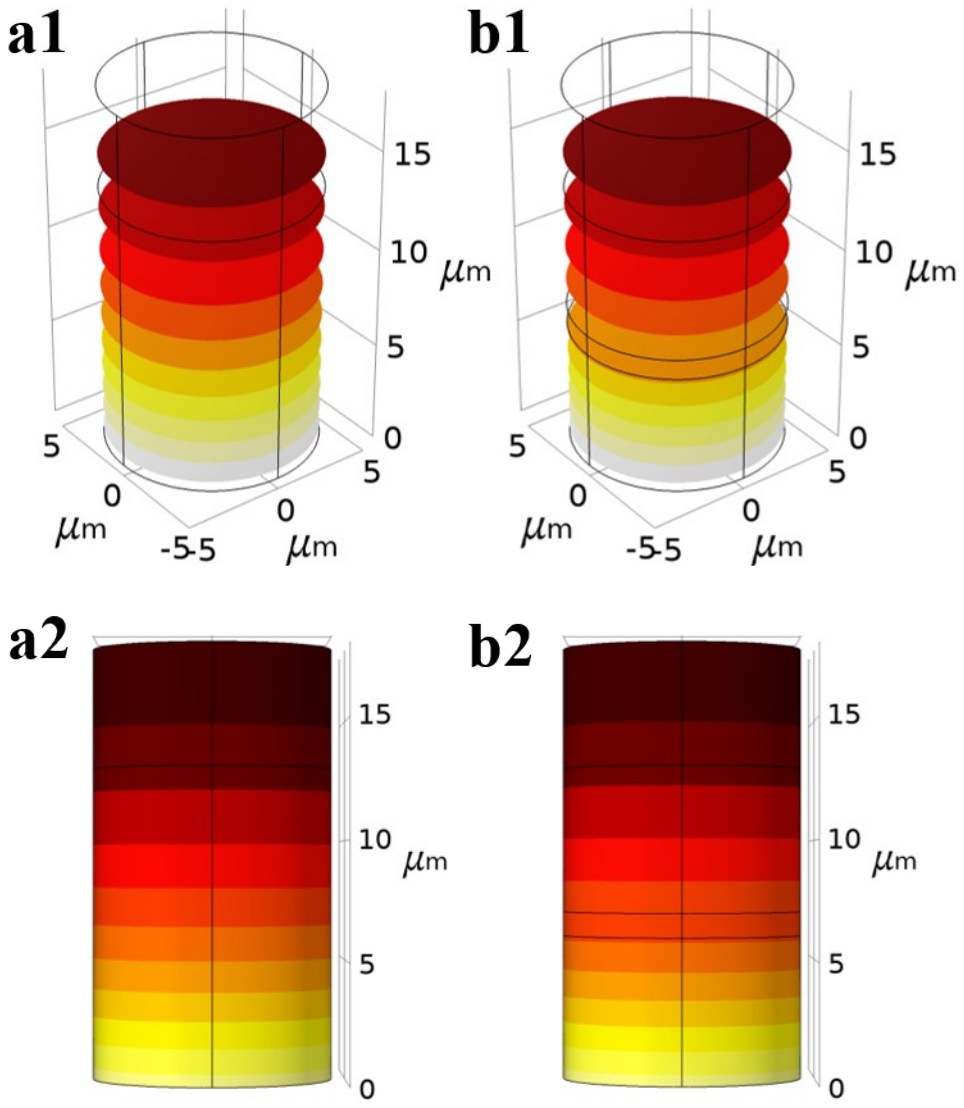

Fig. S17 Isotermal surface distribution of (a) F-E and (b) F-EB_5 composites.

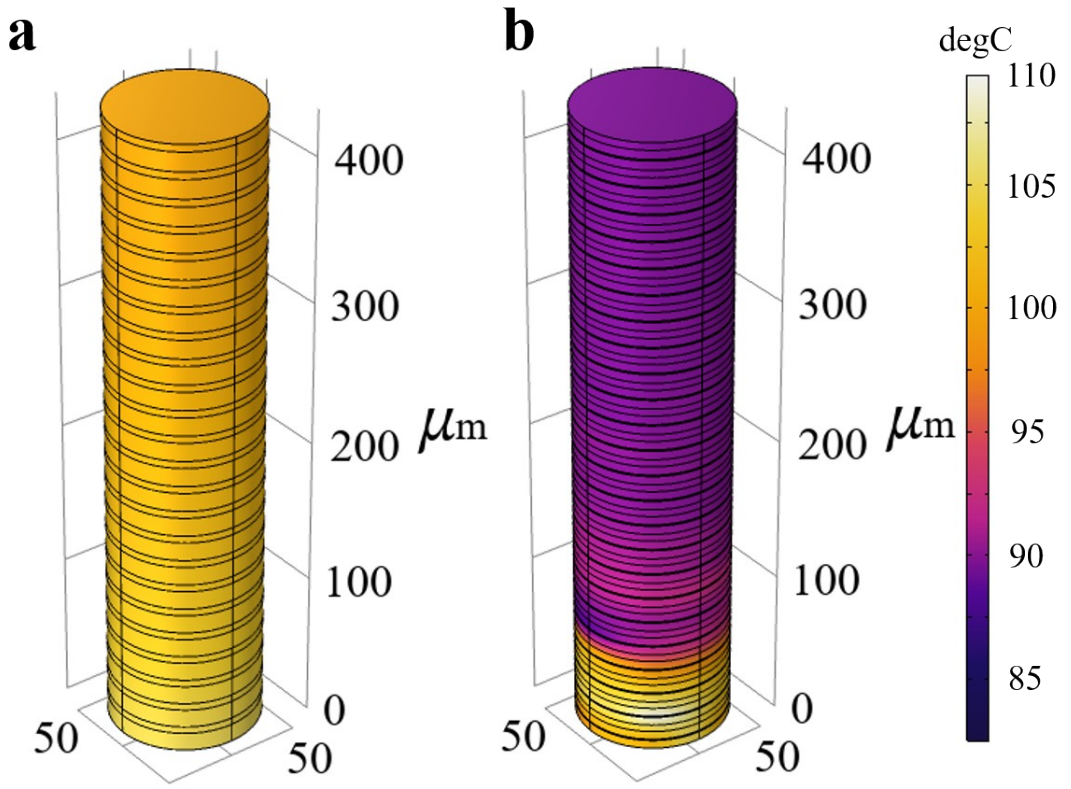

Fig. S18 Heat transfer modelling of multilayer overlap (24 layers) in (a) F-E and (b) F-EB_5 composites.